ACS OMEGA

http://pubs.acs.org/journal/acsodf

Article

Surface Modification by Amino Group Inducing for Highly Efficient Catalytic Oxidation of Toluene over a Pd/KIT-6 Catalyst

Jinglei Cui,* Dan Ren, Jingjing Tan, Huirong Zhang, Yanxia Guo,* and Long Huang*

Cite This: *ACS Omega* 2022, 7, 39950−39958

Read Online

ACCESS | Metrics & More | Article Recommendations | Supporting Information

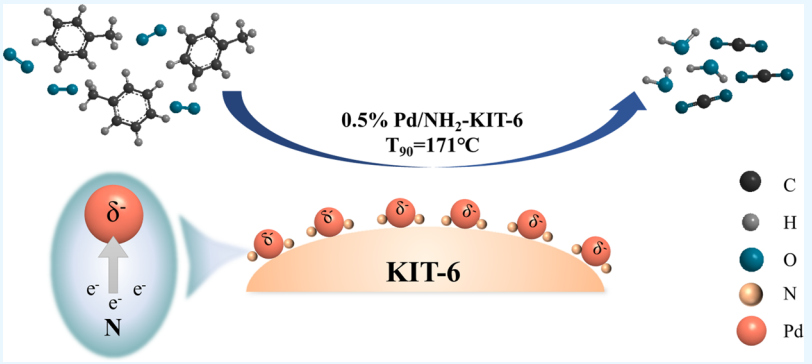

ABSTRACT: Toluene is one of the typical volatile organic compounds in industry, particularly in energy and fuels production processes, which is required to be eliminated effectively to protect the environment. Catalytic oxidation of toluene is widely studied for its high efficiency, and rational design and synthesis of metal catalysts are keys for toluene oxidation. In this study, an efficient catalyst was designed and synthesized by introducing $-NH_2$ groups on the ordered mesoporous silica (KIT-6) surface to anchor and disperse Pd species, leading to Pd nanoparticles being highly dispersed with uniform particle size distribution. Meanwhile, it was found that the introduction of $-NH_2$ made Pd centers present an electron-rich state, and the active Pd centers could activate O_2 molecules to generate more reactive oxygen species and promote the conversion of toluene, which was verified by *in situ* XPS and O_2-TPD characterization. Compared with the catalysts prepared by an impregnation method, the catalytic performance of the Pd/NH_2-KIT-6 (0.5 wt %) catalyst was significantly improved. A conversion of 90% for toluene (2400 ppm, 24,000 $mL{\cdot}g^{-1}{\cdot}h^{-1}$) was achieved at 171 °C, and the toluene conversion was maintained above 90% for 900 min, displaying the excellent activity and stability of the Pd/NH_2-KIT-6 catalyst.

1. INTRODUCTION

Volatile organic compounds (VOCs) include a series of carbon-containing compounds participating in atmospheric photochemical reactions.[1,2] VOCs have relatively high vapor pressures and are therefore prone to evaporation under environmental conditions. VOCs cause air pollution, such as photochemical smog, ground ozone, sick housing syndrome, and chemical sensitivity, which is a serious threat to human health and the environment.[3−6] Toluene is a typical VOC and an aromatic hydrocarbon of benzene ring type. It comes from the process of extracting gasoline and other fuels from crude oil and turning coal into coke, which has obvious environmental hazards.[7]

A few effective technologies have been employed to remove VOCs from pollutant gas.[8] Controlling the generation of VOCs from their sources is the fundamental way to reduce VOC pollution, including clean production and raw material replacement.[9] However, a large number of VOCs are still emitted in the industrial production process, so it is critical to adopt an end treatment technology. Currently, adsorption, membrane separation, regenerative combustion, photocatalysis, plasma technology, and catalytic oxidation have been applied for VOC elimination. Among them, catalytic oxidation is one of the most effective methods to eliminate VOCs for its low operating temperature, no secondary pollution, and high purification efficiency.[10]

Toluene is stable and it is difficult to degrade under natural conditions. Therefore, developing an efficient catalytic system is required for catalytic oxidation of toluene. Noble metal catalysts, such as Pt, Pd, Au, Ag, and Ru, are studied for catalytic oxidation due to their high activity and stability in a high temperature and corrosive reaction process. The d-

Received: July 8, 2022
Accepted: October 14, 2022
Published: October 27, 2022

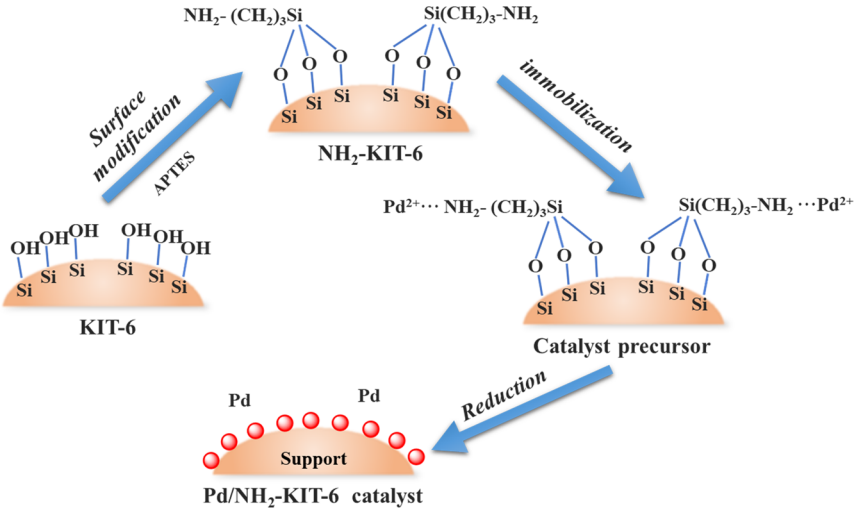

Figure 1. Preparation procedure of the Pd/NH_2-KIT-6 catalyst.

electron orbitals of these noble metals are not fully filled, and the active sites on the surface tend to adsorb reactants, which are conducive to the formation of intermediate active compounds.[11] Pd-supported catalysts are often used to treat benzene series, methane, and other VOCs.[12] Compared with other noble metal catalysts, Pd-based catalysts have a higher heat resistance and hydrothermal resistance in catalytic oxidation of toluene.[8] Typically, the activity of industrial Pd-based catalysts largely depends on the loading amount of Pd. However, noble metals are expensive and their resource is reduced markedly. Therefore, improving the dispersity and utilization rate of active metal will reduce the loading amount of precious metal.[13] Hussain et al. synthesized Pd/SBA-15 catalysts with different Pd loadings (0.25−0.7 wt %) by an impregnation method for catalytic oxidation of methane. The 1−5 nm PdO nanoparticles were evenly dispersed on the surface of SiO_2, leading to a high reaction efficiency for catalytic oxidation.[14] Liu et al. prepared a few Pd/mesoporous silica catalysts by an acetic acid impregnation method, and KIT-6 with a three-dimensional mesoporous structure improved the dispersity of Pd, thus elevating the catalytic activity in selective oxidation of glyoxal.[15] The physicochemical properties of supports play an important role in a highly efficient catalyst. A suitable support can disperse metal sites on the surface, leading to a strong interaction between the support and active sites, thus increasing the activity and stability of catalysts. Ordered mesoporous silica (KIT-6) has a high specific surface area and ordered and flexible pore structure, favoring the dispersion of active metal species.[15,16] Its unique three-dimensional cross-linked pore structure facilitates the dispersion of active substances, which enables reactants and products to migrate rapidly in the pores and avoids blockage.[17]

Pd-based catalysts are typically prepared by an impregnation method in industry since they are easy to operate, and the interaction between the metal and support in these catalysts is mainly van der Waals forces, electrostatic adsorption, or weak covalent bond. The dispersity and stability of the active metal centers are hard to regulate in catalysts.[18] To solve the problem, He et al. synthesized the Pd/ZSM-5/KIT-6 catalyst by a recrystallization method, where Pd species were anchored through a strong interaction with acid sites. The active sites of the catalyst were a mixture of Pd^0 and Pd^{2+}, and the hydrothermal stability of the catalyst was controlled by adjusting the Si/Al mole ratio.[19] Han et al. prepared Pd/Ce-Zr-O_x catalysts by a co-precipitation method, hydrothermal method, impregnation method, and sol−gel method. The results showed that the catalyst prepared by the co-precipitation method had small particle sizes and more exposed active sites, which was favorable for the catalytic oxidation of toluene. However, a large amount of salt solution and ultrapure water was required to adjust the pH and wash the materials in the preparation process.[20] Hui et al. prepared a Pd/SiO_2-P catalyst by H_2 plasma technology, and the morphology and structure of SiO_2 were maintained and the pore size of SiO_2 increased, which significantly improved the dispersion of Pd nanoparticles and the proportion of Pd^0. Additionally, to prepare catalysts with different Pd amounts, different discharge atmospheres and frequencies were strictly controlled during the treatment process, which limited their large-scale application in industry.[13]

Based on existing research studies, developing a Pd catalyst with high efficiency to reduce the cost of noble metal is required. Meanwhile, a simple and controllable preparation technology for the Pd catalyst is necessary for potential industrial applications. To solve the abovementioned problems, a simple method to design highly efficient Pd-based catalysts was developed with surface amino group inducing and Pd species immobilization in this study (Figure 1). The introduced −NH_2 on the support surface (KIT-6) will complex with Pd^{2+} and reduce remarkably the sintering of Pd nanoparticles in the reduction process. More importantly, most electron-donating N atoms on the catalyst surface prefer electron transfer to active metal sites, which facilitate the reactant activation in the oxidation reaction. Compared with the Pd catalyst prepared by an impregnation method, the Pd-NH_2-KIT-6 catalyst prepared by an immobilization method showed a higher activity, which displayed a promising prospect in the industrial production.

2. EXPERIMENTAL SECTION

2.1. Materials. A poly(ethylene oxide)-poly (propylene oxide)-poly (ethylene oxide) triblock copolymer (P123, AR) was purchased from ALDRICH Chemistry (USA). 3-Aminopropyl triethoxysilane (APTES), *n*-butanol, tetraethyl silicate (TEOS) solution, and palladium nitrate solution (Pd 5 wt %) are analytically pure and were purchased from Shanghai

https://doi.org/10.1021/acsomega.2c04331
ACS Omega 2022, 7, 39950−39958

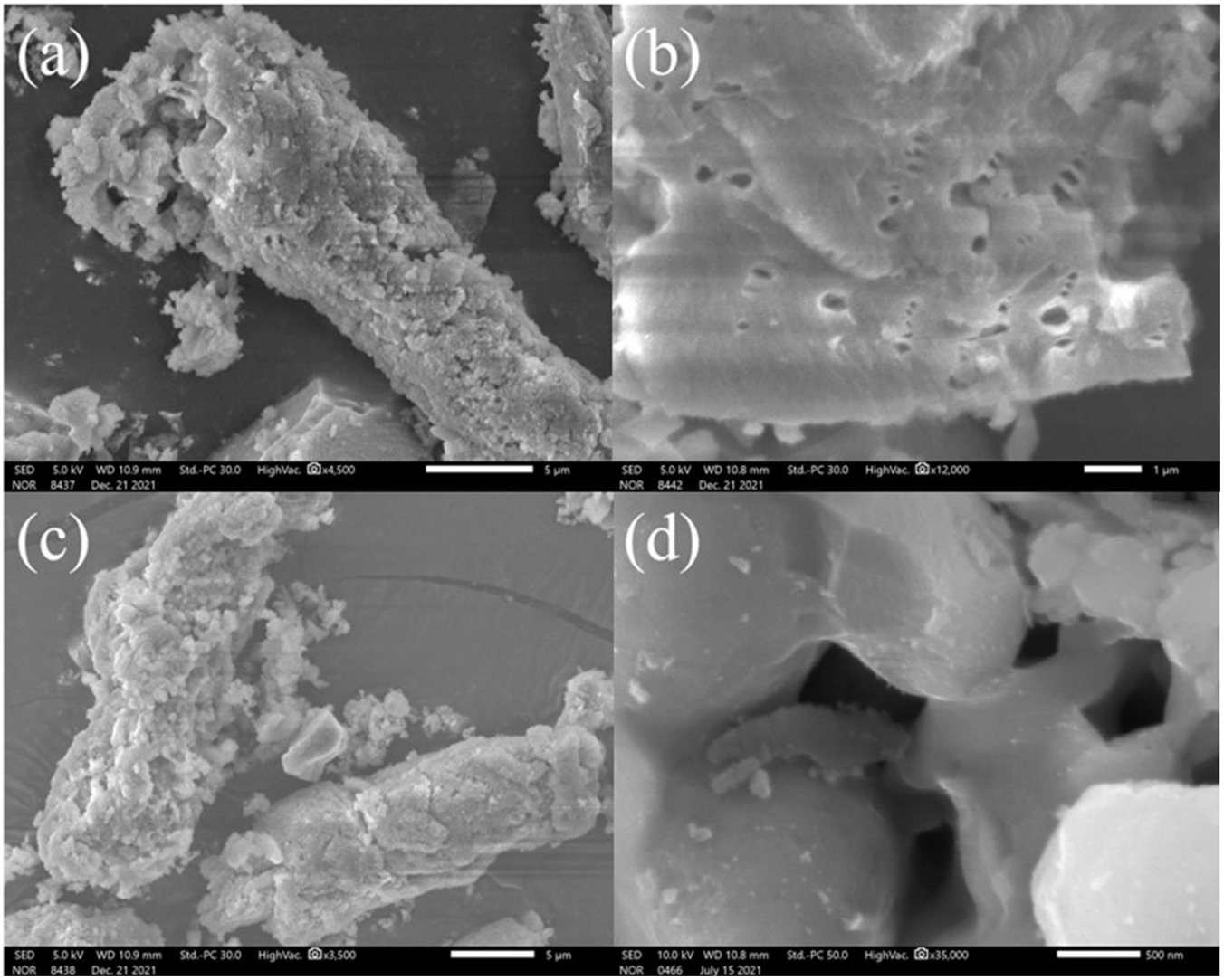

Figure 2. SEM images of KIT-6 (a, b) and NH_2-KIT-6 (c, d).

Aladdin Biochemical Technology Co., Ltd. Toluene (AR), hydrochloric acid (37%), and anhydrous ethanol (AR) were purchased from Sinopharm Chemical Reagent Co., Ltd. All the above reagents were used directly without any pretreatment. Ultrapure water was prepared in the laboratory. N_2 and O_2 (both 99.999%) were purchased from the Gas Department of Shanxi Gangdun Trading Co., Ltd. 5% H_2/Ar mixed gas was purchased from Taiyuan Anxuhongyun Technology Development Co., Ltd.

2.2. Catalyst Preparation. For the synthesis of KIT-6,[21] 4.65 g of P123 was added to the mixed solution of 167.4 g of water and 9.2 g of hydrochloric acid (12 mol/L), and the mixture was stirred magnetically at 35 °C for 4 h. Subsequently, 4.65 g of *n*-butanol was dropped into the mixed solution and stirred magnetically at 35 °C for 1 h. A 10 g TEOS was added into the solution at a speed of 10 r/min by a peristaltic pump, and the system was stirred magnetically at 35 °C for 24 h. Then, the system was transferred to a Teflon tank and aged for 24 h in a 105 °C oven. After that, the material was filtered, washed, and dried to obtain a white powder. The powder was calcined in a muffle furnace at 550 °C for 4 h, and the KIT-6 material was obtained. KIT-6 and anhydrous ethanol were mixed in a round-bottom flask with a solid−liquid ratio of 1:100 (g:mL) and stirred magnetically at room temperature for 30 min. Then, 10 mL of APTES was added and the flask was placed in an oil bath at 70 °C and was refluxed for 24 h. After cooling and filtering, the material was centrifuged, washed with ethanol, and then vacuum-dried at 60 °C for 24 h, and the obtained material was denoted as NH_2-KIT-6.

Pd/KIT-6 catalysts were prepared by an impregnation method. The catalysts were denoted as *x*% IM, where *x* stands for the theoretical amount of Pd in the catalyst. Typically, 0.125 mL of $Pd(NO_3)_2$ (4%) solution was diluted to 2.5 mL with water and 1.0 g of KIT-6 for soaking overnight to obtain the 0.5% IM catalyst. After drying for 24 h in a vacuum drying oven at 40 °C, the catalysts were taken out and calcined at 500 °C for 2 h.

Pd/NH_2-KIT-6 catalysts were prepared by an immobilization method, and the preparation procedures are shown in Figure 1. The catalysts were denoted as *y*% GR, where *y* stands for the theoretical amount of Pd in the catalyst. A 1.0 g NH_2-KIT-6 and 0.125 mL $Pd(NO_3)_2$ (4%) solution were added to 120 mL of anhydrous ethanol and fully mixed in a round-bottom flask. The flask was placed in an oil bath at 70 °C and was refluxed for 24 h to obtain the 0.5% GR catalyst. After

https://doi.org/10.1021/acsomega.2c04331
ACS Omega 2022, 7, 39950−39958

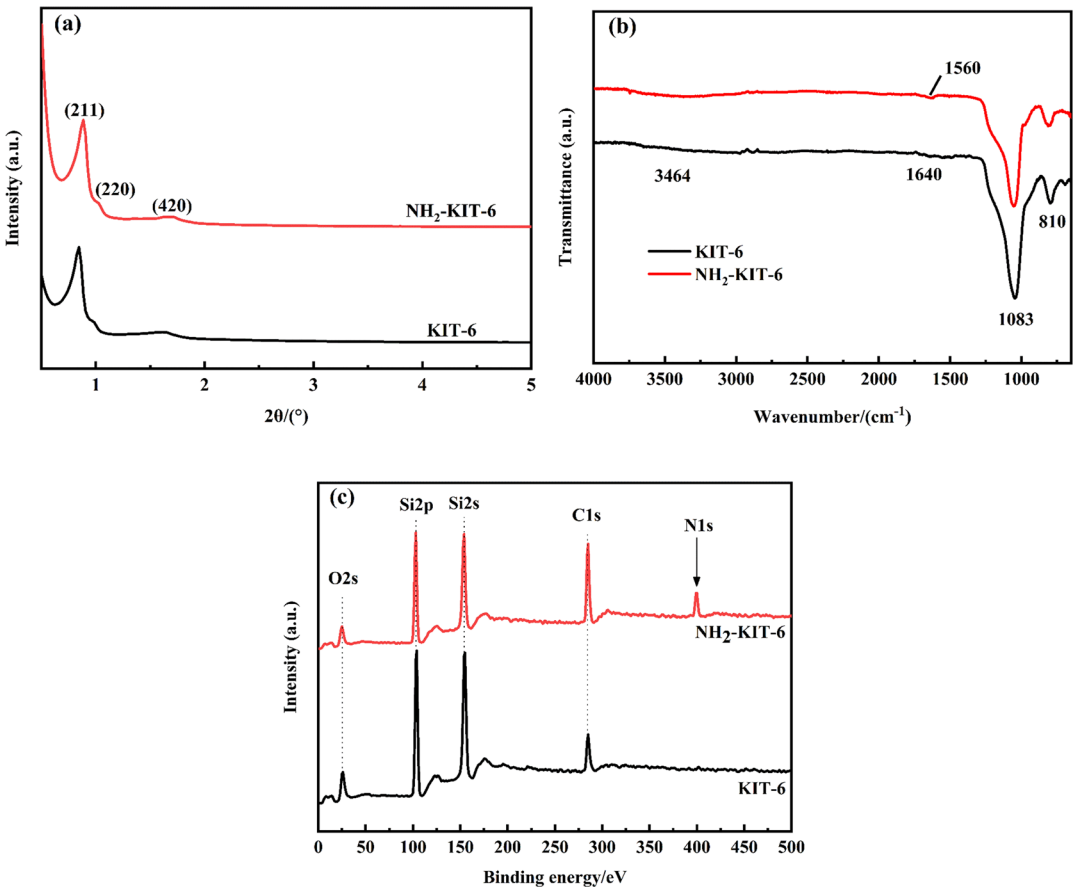

Figure 3. XRD patterns of KIT-6 and NH_2-KIT-6 (a), FTIR spectra of KIT-6 and NH_2-KIT-6 (b), and XPS spectra of KIT-6 and NH_2-KIT-6 (c).

cooling and filtering, the material was centrifuged and washed with anhydrous ethanol twice and then vacuum-dried at 80 °C for 24 h.

2.3. Catalyst Evaluation. Catalyst evaluation was performed in a fixed-bed reactor with a diameter of 8 mm (as seen in Figure S1, in the Supporting Information). N_2 was pumped into a toluene bubbler soaked in an ice water bath for bubbles. The O_2 content was 20%, and N_2 was the equilibrium gas. Before the catalytic reaction, 0.2 g of catalyst (20−40 mesh) and 0.8 g of quartz (20−40 mesh) were mixed and loaded into the reaction tube and then reduced at 300 °C (IM catalyst) or 500 °C (GR catalyst) in a 5% H_2/Ar atmosphere (40 mL/min) for 2 h in the fix-bed reactor.

The mass space velocity (WHSV) was 24,000 $mL{\cdot}g^{-1}{\cdot}h^{-1}$. The toluene concentration in reaction tail gas was analyzed online by gas chromatography (Zhongke Huifen GC-7820) with an FID detector, and the CO_2 concentration was detected by another FID detector with a conversion furnace to convert CO_2 to CH_4. During the catalyst evaluation, the catalyst bed temperature was raised to 120 °C for the first time and kept for 30 min. Then, the heating rate was raised to the next temperature at 3 °C/min. After reaching the temperature for 20 min, the toluene content in tail gas was determined. Toluene conversion ($X_{toluene}$%) could be calculated by the following formula:

$$X_{toluene}\% = \frac{[toluene]_{in} - [toluene]_{out}}{[toluene]_{in}} \times 100\%$$

where $[toluene]_{in}$ and $[toluene]_{out}$ represent the inlet and outlet concentrations of toluene in tail gas, respectively. Typically, the catalytic performance of the catalysts was compared with the temperature (T_x) when the conversion of toluene was x%.

3. RESULTS AND DISCUSSION

3.1. Surface Modification of KIT-6. Figure 2 shows the SEM images of KIT-6 (Figure 2a,b) and NH_2-KIT-6 (Figure 2c,d). It was found that KIT-6 had curved rod-like morphology before and after modification. KIT-6 and the modified NH_2-KIT-6 were characterized by small-angle XRD, and the results are shown in Figure 3a. It could be seen that there were clear diffraction peaks of (211), (220), and (420), which were the typical double continuous cubic structure of KIT-6. This result indicated that the mesoporous silica KIT-6 was successfully prepared. After modification, three crystal plane diffraction peaks of KIT-6 were still clearly visible, indicating that the structural order of KIT-6 was retained after modification. The changes of functional groups on the surface of KIT-6 and NH_2-KIT-6 could be observed in the ATR-FTIR spectra (Figure 3b). The characteristic band of 3464 cm^{-1} represents the stretching vibration of a hydrogen-bonded silanol group (Si−OH). The band at 1640 cm^{-1} was the O−H bending vibration of physically adsorbed water molecules.[22] Before and after modification, the anti-symmetric and symmetric stretching vibration of the Si−O−Si bond both appeared in KIT-6 at 1083 and 810 cm^{-1} with strong peak strength, respectively.[23] The characteristic band of 1560 cm^{-1} only existed in the FTIR spectrum of NH_2-KIT-6, which was the bending vibration of a N−H bond. Figure 3c shows the full XPS spectra of KIT-6 and NH_2-KIT-6, and the additional signal of N was observed in the

https://doi.org/10.1021/acsomega.2c04331
ACS Omega 2022, 7, 39950−39958

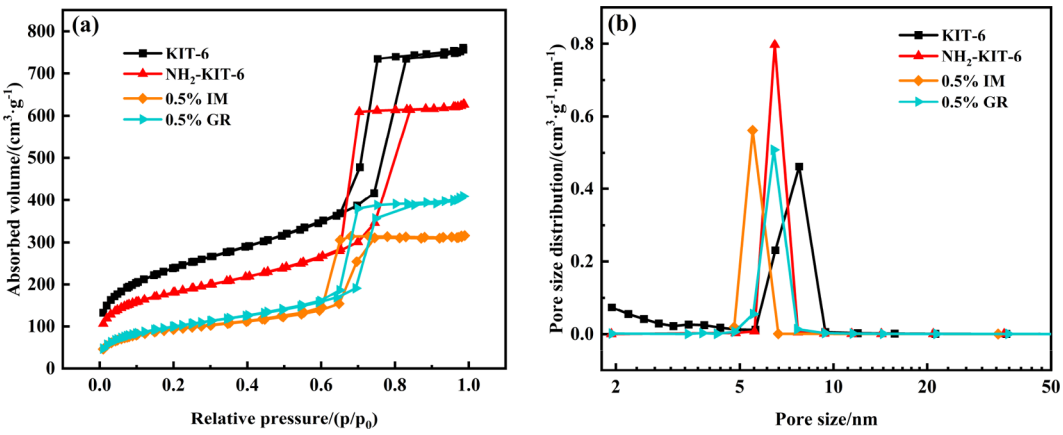

Figure 4. N_2 adsorption/desorption isotherms (a) and pore size distributions (b) of the catalysts.

spectrum of NH_2-KIT-6. These results indicated that aminosilane was successfully bound to the surface of KIT-6 by modification.

3.2. Characterizations of Catalysts. *3.2.1. N_2 Physical Adsorption/Desorption.* Figure 4 shows the N_2 adsorption/desorption isotherms (Figure 4a) and pore size distributions (Figure 4b) for the supports and catalysts. All samples showed characteristic type IV curves of the isotherms with an H1 type hysteresis loop according to the IUPAC definition. The pore size distributions of the catalysts were uniformly concentrated in 5−10 nm. The pore size of mesopores in catalysts was slightly reduced compared with the KIT-6 support, which was likely due to the active metal PdO nanoparticles introduced into the internal channels of KIT-6.

Table 1 summarizes the specific surface area, pore parameters, and Pd dispersion of the catalysts. The KIT-6 support had a high specific surface area and a pore volume. Both the specific surface area and pore volume of KIT-6 decreased after loading Pd by an impregnation method. Specifically, the specific surface area and pore volume of NH_2-KIT-6 decreased significantly after surface modification, which was caused by the grafting of a 3-aminopropyl group into the pores of KIT-6. Additionally, the Pd dispersion of the 0.5%GR catalyst was much higher than that of the 0.5% IM catalyst, displaying that the introduction of $-NH_2$ on the surface of KIT-6 greatly improved the dispersity of Pd species in the reduction process.

Table 1. Texture Properties of the Catalysts

samples	Pd (wt %)[a]	S_{BET} (m^2/g)	V_p (cm^3/g)	d_p (nm)	Pd dispersion
KIT-6		842	1.16	5.49	
NH_2-KIT-6		327	0.48	5.88	
0.5% IM	0.49	629	0.96	6.09	28%
0.5% GR	0.48	360	0.61	6.80	51%

[a]The content of Pd was determined by ICP-OES.

3.2.2. XRD Characterization. Figure 5 shows the XRD pattern of the catalysts. The wide peak around 23° was the diffraction peak of amorphous silica.[24] The diffraction peak of PdO centered at 32° appeared in the 0.5% IM catalyst, indicating that large PdO particles were formed in the channel of the KIT-6 support. The interaction of Pd species and KIT-6 was weak in the IM catalyst, which would lead to aggregation of PdO in the calcination process. There was no diffraction peak of PdO in the catalyst prepared by an immobilization method, which indicated that Pd^{2+} combined with the $-NH_2$ grafted in the surface of KIT-6 through coordination complexation, improving the dispersity of Pd species.

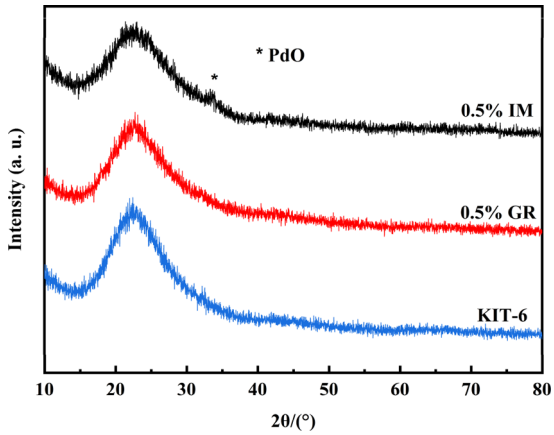

Figure 5. XRD patterns of catalysts.

3.2.3. TEM Characterization. Transmission electron microscopy was applied to characterize the morphology of the 0.5% IM (Figure 6a,c) and 0.5% GR (Figure 6b,d) catalysts. It was observed that KIT-6 had regularly ordered channels (Figure S2, in the Supporting Information), which displayed a long-range ordered three-dimensional structure. After introducing Pd, an ordered pore structure was clearly observed in the 0.5% IM and 0.5% GR catalysts, indicating that the ordered structure was stable in the preparation process. Moreover, Pd nanoparticles agglomerated obviously in the 0.5% IM catalyst, while Pd nanoparticles dispersed uniformly on the surface of the 0.5% GR catalyst. The particle size of Pd nanoparticles on the 0.5% GR catalyst was around 2 nm (Figure 6f), while the particle size of Pd nanoparticles on the 0.5% IM catalyst was larger and mainly concentrated in 5−8 nm (Figure 6e). These results verified that the introduction of $-NH_2$ group inhibited further aggregation of Pd particles during the reduction process, which significantly enhanced the dispersion of Pd nanoparticles on the catalyst surface.

3.2.4. XPS Characterization. To study the structure and chemical environment of different Pd-based catalysts, *in situ* XPS was applied to characterize the two catalysts, and the results are shown in Figure 7 and Figure S3 (in the Supporting Information). The N signal of the 0.5% GR catalyst had a

https://doi.org/10.1021/acsomega.2c04331
ACS Omega 2022, 7, 39950−39958

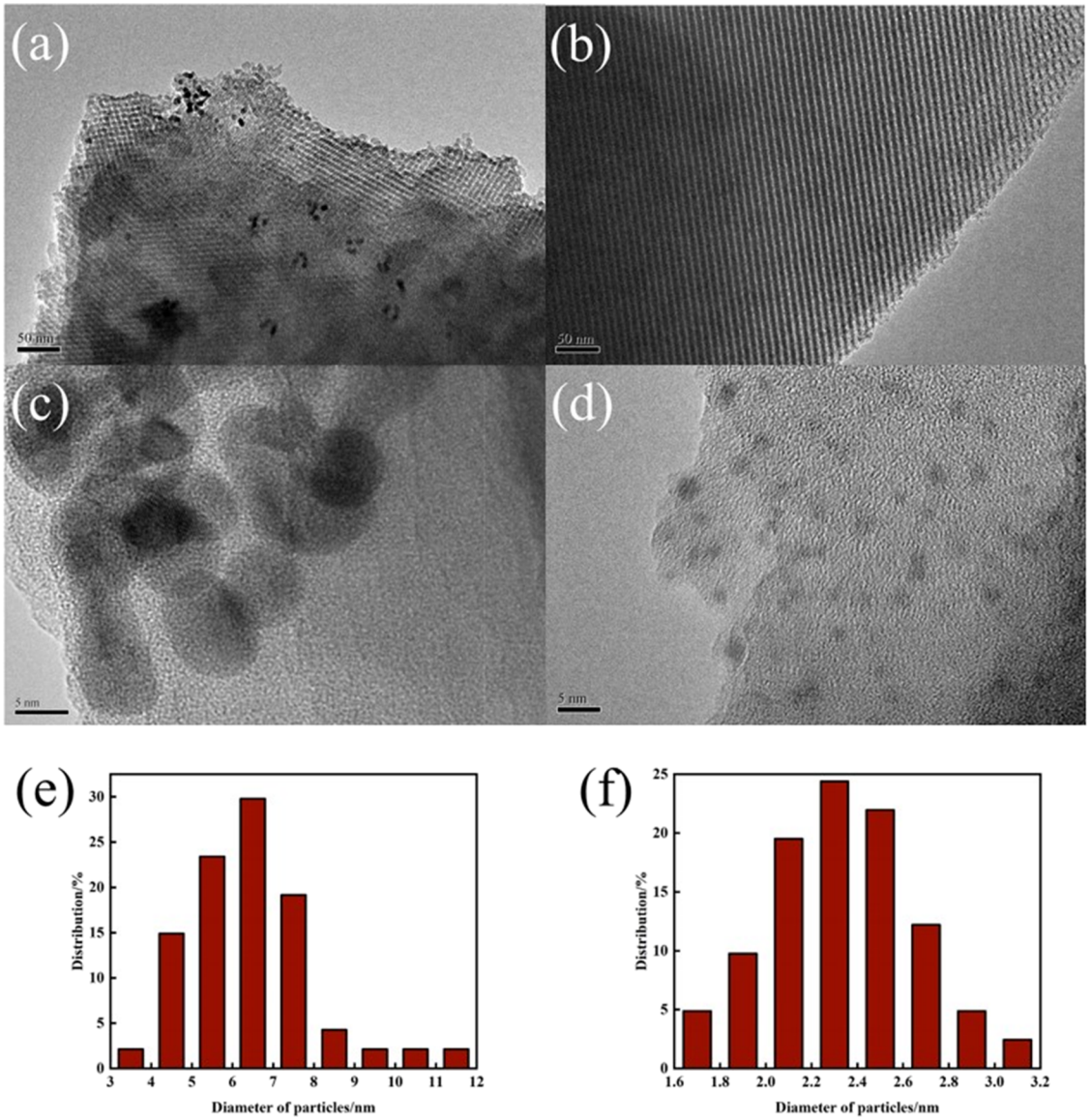

Figure 6. TEM images and Pd particle size distribution of 0.5% IM (a, c, e) and 0.5% GR catalyst (b, d, f).

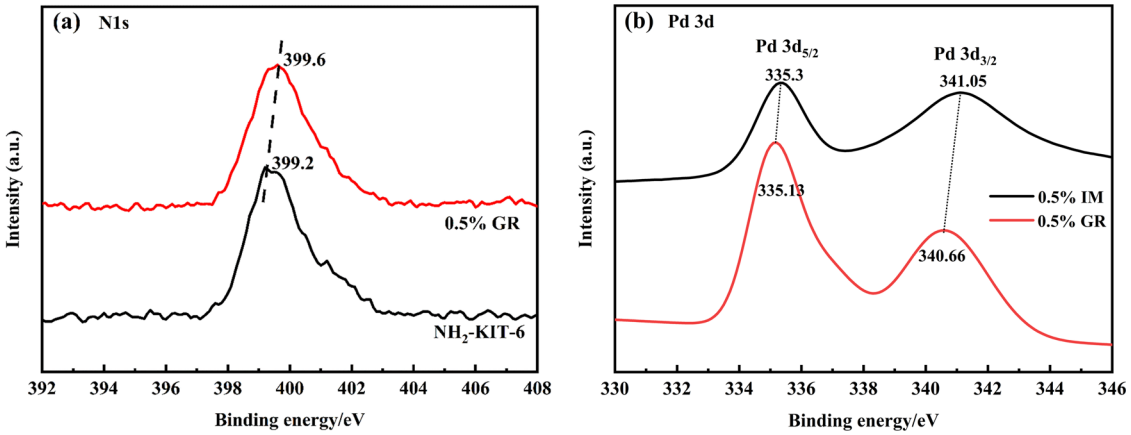

Figure 7. XPS spectra of N 1s in NH_2-KIT-6 and 0.5% GR catalysts (a). XPS spectra of Pd 3d in the 0.5% IM catalyst and 0.5% GR catalyst (b).

positive shift of 0.4 eV compared with that of the NH_2-KIT-6 support (Figure 7a). Additionally, Pd^0 $3d_{5/2}$ (335.3 eV) had a negative shift of 0.17 eV and Pd^0 $3d_{3/2}$ (341.05 eV) had a negative shift of 0.39 eV for the 0.5% GR catalyst compared with the 0.5% IM catalyst. These results indicated that electrons were transferred from N to Pd^0, leading to Pd^0 in the

https://doi.org/10.1021/acsomega.2c04331
ACS Omega 2022, 7, 39950−39958

0.5% GR catalyst showing an electron-rich state. The rate-controlling step for toluene degradation was the cleavage of the C−C bond of the benzene ring and the conversion of benzoate to maleic anhydride, which required a large amount of reactive oxygen species.[25] The Pd^0 species with an electron-rich state could activate electrophilic O_2 molecules, thereby generating more reactive oxygen species. Under oxygen-enriched conditions, sufficient reactive oxygen species ensured the continuous degradation of toluene and the accumulation of intermediates.[26]

3.2.5. O_2-TPD Characterization. To further investigate the nature of adsorbed and activated oxygen species that would participate in the oxidation of toluene, O_2-TPD was performed and the results are shown in Figure 8. Three peaks were

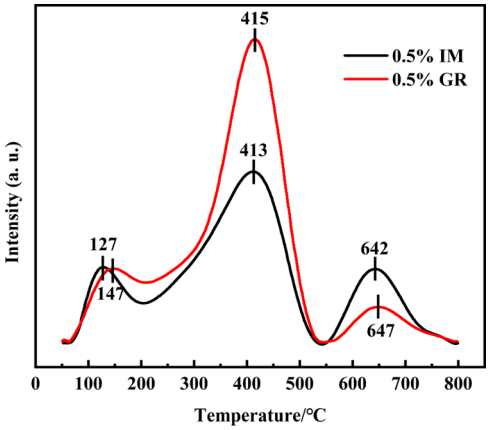

Figure 8. O_2-TPD profiles of the catalysts.

observed for the 0.5% IM and 0.5% GR catalyst. The peaks centered at 127 and 147 °C for 0.5% IM and 0.5% GR catalysts were assigned to the desorption of molecular oxygen O_2^- ($O_2^-{}_{ad}$).[27] The desorption peaks centered at a temperature of 415 or 417 °C belong to the chemically adsorbed O^- ($O^-{}_{ad}$) on the surface of the catalyst.[28] These surface oxygen species were active and could promote the catalytic reactivity for toluene oxidation; among them, $O_2^-{}_{ad}$ is more active than $O^-{}_{ad}$ for the oxidation reaction.[29] Other peaks centered at 642 or 647 °C were observed, which were attributed to the release of bulk phase lattice O^{2-} ($O^{2-}{}_{lat}$), and the $O^{2-}{}_{lat}$ species was inactive in toluene oxidation. Compared with the 0.5% IM catalyst, the total amount of desorbed oxygen species obtained by the peak area was higher for the 0.5% GR catalyst (Table S1, in the Supporting Information). Specifically, much more reactive surface oxygen ($O^{2-}{}_{ad}$ and $O^-{}_{ad}$) was found for the 0.5% GR catalyst. These results displayed that the 0.5% GR catalyst owned a better capability for O_2 activation in the reaction, facilitating the supply and supplementing the active oxygen species and therefore improving catalytic efficiency for toluene oxidation. The highly dispersed Pd in the 0.5% GR catalyst played an important role in the absorption and activation of O_2. Meanwhile, surface Pd of the 0.5% GR catalyst is in the electron-rich state (as seen in Figure 7b), which will facilitate the activation of electrophilic O_2 molecules, thereby generating more reactive oxygen species.[26] Therefore, the higher amount of surface $O_2^-{}_{ad}$ and $O^-{}_{ad}$ on the GR catalyst is likely due to the combined effect of high dispersion of Pd and the electron-rich state of surface Pd^0 in the 0.5% GR catalyst.

3.3. Catalytic Evaluation. Figure 9 shows the toluene conversion curves of 0.5% IM and 0.5% GR catalysts, and the

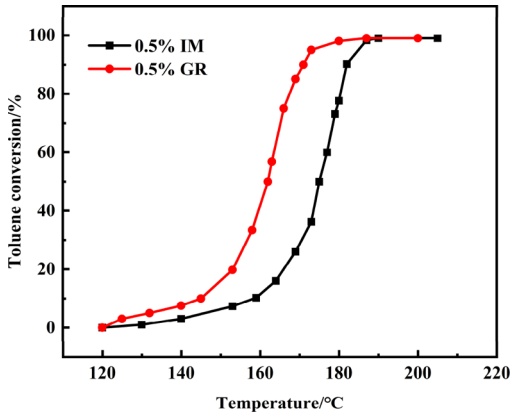

Figure 9. Toluene conversion curves of 0.5% IM and 0.5% GR catalysts.

detailed data are shown in Table S2 (Supporting Information). The catalytic conversion of toluene was observed above 120 °C over the two catalysts, and toluene conversion increased with the increase in reaction temperature. During the reaction, no other byproducts except CO_2 were detected. The reaction temperatures for 10, 50, 75,and 90% conversion of toluene over the 0.5% GR catalyst were lower than those over the 0.5% IM catalyst, displaying the higher activity of the 0.5% GR catalyst. Specifically, the T_{90} of the 0.5% GR catalyst was 171 °C, while the same conversion was observed at 182 °C for the 0.5% IM catalyst. In addition, the 0.5% GR catalysts prepared in this study showed a higher catalytic activity compared to other Pd-based catalysts reported in the literature (Table 2).

Table 2. Comparison of Catalysts in This Study and the Literature

catalyst	toluene concentration	space velocity	T_{90} (°C)
0.5% GR (this study)	2400 ppm	24,000 mL g^{-1} h^{-1}	171
0.5% Pd/Mn_3Ce_2-300[30]	1000 ppm	30,000 mL g^{-1} h^{-1}	185
$Pd/MgO\text{-}Al_2O_3$[31]	500 ppm	24,000 mL g^{-1} h^{-1}	209
0.5% Au-0.27 %Pd/CeO_2/GC[32]	314 ppm	30,600 h^{-1}	175
0.5% Pd/MCM-41[33]	1000 ppm	50,400 mL g^{-1} h^{-1}	230
0.92% $Pd/InO_x@CoO_x$[34]	3000 ppm	30,000 mL g^{-1} h^{-1}	253

Meanwhile, it was found that the turnover frequency (TOF) of the 0.5% GR catalyst was much higher than that of the 0.5% IM catalyst (as seen in Table S1, in the Supporting Information). The introduction of $-NH_2$ avoided the sintering of Pd species in the 0.5% GR catalyst, therefore a high dispersity was achieved by the immobilization methods, and the high Pd dispersion greatly improved the catalytic efficiency for the oxidation of toluene. More importantly, compared with the 0.5% IM catalyst, the surface Pd^0 is in an electron-rich state, which transfers from the N on the catalyst surface (as seen in Figure 7). These surface Pd^0 of the 0.5% GR catalyst are more active for the absorption and activation of molecular O_2, which likely resulted in a higher TOF value in the toluene conversion.

The effect of space velocity (WHSV) on catalyst activity was studied over the 0.5% GR catalyst (Figure 10a and Table S3).

https://doi.org/10.1021/acsomega.2c04331
ACS Omega 2022, 7, 39950−39958

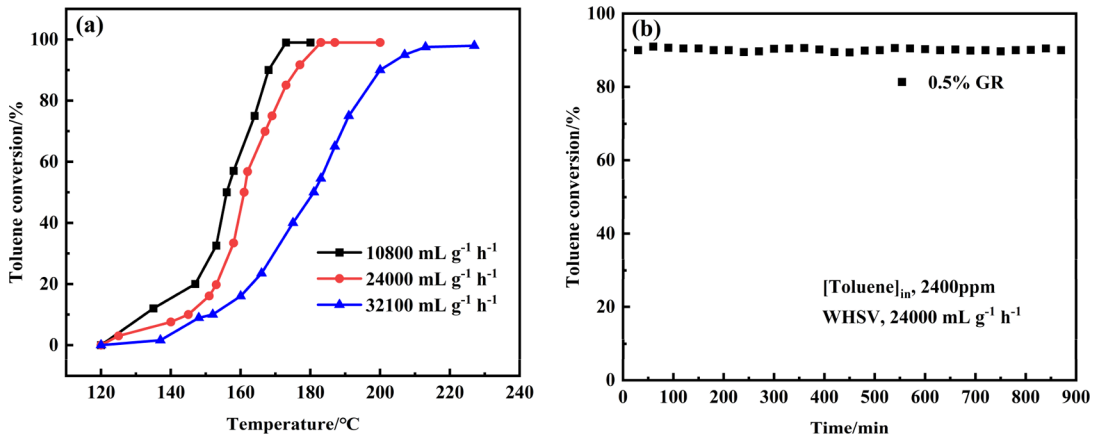

Figure 10. Effect of WHSV on the toluene conversion (a). Stability test of the catalyst (b).

The catalytic activity of 0.5% GR increased with decreasing WHSV. When the WHSV decreased from 24,000 to 10,800 $mL{\cdot}g^{-1}{\cdot}h^{-1}$, the T_{50} and T_{90} decreased from 162 and 171 °C to 156 and 168 °C, respectively. When the WHSV increased from 24,000 to 32,100 $mL{\cdot}g^{-1}{\cdot}h^{-1}$, the T_{50} and T_{90} increased from 162 and 171 °C to 181 and 200 °C, respectively. The results showed that reducing the WHSV and increasing the contact time between the catalyst and reaction gas could improve the conversion efficiency of toluene catalytic oxidation.

The stability of the catalyst is important to measure its comprehensive performance. The stability of the 0.5% GR catalyst was tested at 171 °C (Figure 10b). It could be found that the conversion of toluene remained at a high level and no obvious loss in activity was observed for 900 min, displaying the favorable stability of the catalyst. The XRD, XPS, and TEM results of 0.5% GR after catalytic cycles are provided in Figure S6 in the Supporting Information. No obvious aggregation of Pd nanoparticles was found. Meanwhile, part of Pd^0 has transformed into PdO and PdO_2 after the oxidation reaction, which was found in the XRD and XPS results (Figure S6).

4. CONCLUSIONS

Pd/KIT-6 catalysts were synthesized by an immobilization method and impregnation method. The catalysts were characterized by a series of characterization methods including XRD, BET, FT-IR, TEM, *in situ* XPS, and O_2-TPD. It could be found that the Pd nanoparticles prepared by the immobilization method had a better dispersion. XPS and O_2-TPD results verified electron-rich Pd^0 could activate O_2 molecules to generate more reactive oxygen species, which in turn promoted the conversion of toluene. The catalytic activity test also showed that the catalysts prepared by the immobilization method had a higher catalytic activity. The excellent catalytic performance of the catalyst was due to the introduction of the $-NH_2$ groups on the KIT-6 support, inducing the formation of highly dispersed nano Pd active center on the catalyst. The stability test showed that the 0.5 wt % Pd/NH_2-KIT-6 catalyst had no obvious deactivation within the reaction for 900 min.

ASSOCIATED CONTENT

Supporting Information

The Supporting Information is available free of charge at https://pubs.acs.org/doi/10.1021/acsomega.2c04331.

Diagram of catalyst activity evaluation device (Figure S1); characterizations (Figures S2, S3, S4, S5, and S6); and other experiments (Tables S1, S2, and S3) (PDF)

AUTHOR INFORMATION

Corresponding Authors

Jinglei Cui − *Yellow River Laboratory of Shanxi Province, Institute of Resources and Environmental Engineering, Shanxi University, Taiyuan 030006, PR China*; orcid.org/0000-0001-9478-1378; Email: cuijl@sxu.edu.cn

Yanxia Guo − *Yellow River Laboratory of Shanxi Province, Institute of Resources and Environmental Engineering, Shanxi University, Taiyuan 030006, PR China*; Email: guoyx@sxu.edu.cn

Long Huang − *Beijing Key Laboratory of Fuels Cleaning and Advanced Catalytic Emission Reduction Technology, Beijing Institute of Petrochemical Technology, Beijing 102617, China*; Email: huangl@bipt.edu.cn

Authors

Dan Ren − *Yellow River Laboratory of Shanxi Province, Institute of Resources and Environmental Engineering, Shanxi University, Taiyuan 030006, PR China*

Jingjing Tan − *Engineering Research Center of Ministry of Education for Fine Chemicals, Shanxi University, Taiyuan 030006, PR China*; orcid.org/0000-0002-2118-0560

Huirong Zhang − *Yellow River Laboratory of Shanxi Province, Institute of Resources and Environmental Engineering, Shanxi University, Taiyuan 030006, PR China*; orcid.org/0000-0002-7123-749X

Complete contact information is available at: https://pubs.acs.org/10.1021/acsomega.2c04331

Notes

The authors declare no competing financial interest.

ACKNOWLEDGMENTS

The authors gratefully acknowledge the financial support by the National Key R&D Program of China (2020YFB0606402) and the Basic Research Program of Shanxi Province, China (202103021224008).

REFERENCES

(1) Wang, J.; Wang, X.; Liu, X.; Zhu, T.; Guo, Y.; Qi, H. Catalytic oxidation of chlorinated benzenes over V_2O_5/TiO_2 catalysts: The effects of chlorine substituents. *Catal. Today* **2015**, *241*, 92−99.

(2) Wang, J.; Liu, X.; Zeng, J.; Zhu, T. Catalytic oxidation of trichloroethylene over TiO_2 supported ruthenium catalysts. *Catal. Commun.* **2016**, *76*, 13−18.

(3) Magureanu, M.; Dobrin, D.; Mandache, N. B.; Cojocaru, B.; Parvulescu, V. I. Toluene oxidation by non-thermal plasma combined with palladium catalysts. *Front. Chem.* **2013**, *1*, 7.

(4) Odoom-Wubah, T.; Li, Q.; Wang, Q.; Usha, M. Z. R.; Huang, J.; Li, Q. Template-free synthesis of carbon self-doped ZnO superstructures as efficient support for ultra fine Pd nanoparticles and their catalytic activity towards benzene oxidation. *Mol. Catal.* **2019**, *469*, 118−130.

(5) Liang, X.; Chen, X.; Zhang, J.; Shi, T.; Sun, X.; Fan, L.; Wang, L.; Ye, D. Reactivity-based industrial volatile organic compounds emission inventory and its implications for ozone control strategies in China. *Atmos. Environ.* **2017**, *162*, 115−126.

(6) Li, Y.; Shen, Y.; Niu, Z.; Tian, J.; Zhang, D.; Tang, Z.; Li, W.Process analysis of temperature swing adsorption and temperature vacuum swing adsorption in VOCs recovery from activated carbon. *Chin. J. Chem. Eng.*2022, DOI: 10.1016/j.cjche.2022.01.029.

(7) Xunxun, L.; Dongyun, C.; Najun, L.; Qingfeng, X.; Hua, L.; Jinghui, H.; Jianmei, L. Highly efficient Pd catalysts loaded on $La_{1-x}Sr_xMnO_3$ perovskite nanotube support for low-temperature toluene oxidation. *J. Alloys Compd.* **2021**, *871*, No. 159575.

(8) David, M.; Abubakar, Y.; Yong, S.; Chengjun, W.; Yong, R.; Jungang, L.; Hang, X.; George Zheng, C.; Jun, H. Current progress on catalytic oxidation of toluene: a review. *Environ. Sci. Pollut. Res.* **2021**, *28*, 62030−62060.

(9) Song, S.; Zhang, S.; Zhang, X.; Verma, P.; Wen, M. Advances in Catalytic Oxidation of Volatile Organic Compounds over Pd-Supported Catalysts: Recent Trends and Challenges. *Front. Mater.* **2020**, *7*, 599349.

(10) Zhang, Z.; Jiang, Z.; Shangguan, W. Low-temperature catalysis for VOCs removal in technology and application: A state of the art review. *Catal. Today* **2016**, *264*, 270−278.

(11) Kamal, M. S.; Razzak, S. A.; Hossain, M. M. Catalytic oxidation of volatile organic compounds (VOCs): A review. *Atmos. Environ.* **2016**, *140*, 117−134.

(12) Guo, M.; Li, H.; Ren, Y.; Ren, X.; Yang, Q.; Li, C. Improving Catalytic Hydrogenation Performance of Pd Nanoparticles by Electronic Modulation Using Phosphine Ligands. *ACS Catal.* **2018**, *8*, 6476−6485.

(13) Hui, W.; Yifei, Z.; Mingwei, W.; He, X.; Xiaoyong, J.; Jie, Z.; Zhaoyin, H.Pd/SiO_2 Catalysts Prepared via a Dielectric Barrier Discharge Hydrogen Plasma with Improved Performance for Low-Temperature Catalytic Combustion of Toluene. *Ind. Eng. Chem. Res.***2020**, *59* ().

(14) Hussain, M.; Deorsola, F. A.; Russo, N.; Fino, D.; Pirone, R. Abatement of CH_4 emitted by CNG vehicles using Pd-SBA-15 and Pd-KIT-6 catalysts. *Fuel* **2015**, *149*, 2−7.

(15) Liu, J.; Qin, F.; Huang, Z.; Huang, L.; Liao, Z.; Xu, H.; Shen, W. Selective Oxidation of Glyoxal to Glyoxalic Acid by Air over Mesoporous Silica Supported Pd Catalysts. *Catal. Lett.* **2019**, *149*, 1894−1902.

(16) Christopher, M. A. P.; Duncan, W. B.; Nicole, S. H.; Adam, F. L.; Karen, W. Support-Enhanced Selective Aerobic Alcohol Oxidation over Pd/Mesoporous Silicas. *ACS Catal.* **2011**, *1*, 636−640.

(17) Xuejun, Z.; Peipei, Z.; Hongbo, Y.; Zhen, M.; Shenghu, Z. Mesoporous KIT-6 Supported Pd−M_xO_y (M = Ni, Co, Fe) Catalysts with Enhanced Selectivity for p-Chloronitrobenzene Hydrogenation. *Catal. Lett.* **2015**, *145*, 784−793.

(18) Fan, H.; Tan, J.; Zhu, Y.; Zheng, H.; Li, Y. Efficient hydrogenation of dimethyl oxalate to methyl glycolate over highly active immobilized-ruthenium catalyst. *J. Mol. Catal. A: Chem.* **2016**, *425*, 68−75.

(19) He, C.; Li, J.; Zhang, X.; Yin, L.; Chen, J.; Gao, S. Highly active Pd-based catalysts with hierarchical pore structure for toluene oxidation: Catalyst property and reaction determining factor. *Chem. Eng. J.* **2011**, *180*, 46−56.

(20) Han, W.; Dong, F.; Zhao, H.; Zhang, G.; Tang, Z. Exploring the Influence of Pd Species Valence State and Chemisorbed Oxygen Concentration on the Catalytic Oxidation Performance of Toluene. *Catal. Surv. Asia* **2019**, *23*, 110−125.

(21) Kleitz, F.; Choi, S. H.; Ryoo, R. Cubic Ia3d large mesoporous silica: synthesis and replication to platinum nanowires, carbon nanorods and carbon nanotubes. *Chem. Commun.* **2003**, *17*, 2136−2137.

(22) Ncube, T.; Kumar Reddy, K. S.; Al Shoaibi, A.; Srinivasakannan, C. Benzene, Toluene, m-Xylene Adsorption on Silica-Based Adsorbents. *Energy Fuels* **2017**, *31*, 1882−1888.

(23) Latifi, L.; Sohrabnezhad, S. Influence of pore size and surface area of mesoporous silica materilas (MCM-41 and KIT-6) on the drug loading and release. *J. Sol-Gel Sci. Technol.* **2018**, *87*, 626−638.

(24) Shiling, Z.; Jingxuan, C.; Qiumei, H.; Danyang, Z.; Jianyi, S. Microcalorimetric adsorption and infrared spectroscopic studies of supported Pd, Ru and Pd-Ru catalysts for the hydrogenation of aromatic rings with carboxyl groups. *Catal. Sci. Technol.* **2021**, *11*, 3070−3083.

(25) Liao, Y.; Zhang, X.; Peng, R.; Zhao, M.; Ye, D. Catalytic properties of manganese oxide polyhedra with hollow and solid morphologies in toluene removal. *Appl. Surf. Sci.* **2017**, *405*, 20−28.

(26) Xiao, M.; Yu, X.; Guo, Y.; Ge, M. Boosting Toluene Combustion by Tuning Electronic Metal-Support Interactions in In Situ Grown Pt@Co_3O_4 Catalysts. *Environ. Sci. Technol.* **2022**, *56*, 1376−1385.

(27) Huang, H.; Ye, X.; Huang, H.; Zhang, L.; Leung, D. Y. C. Mechanistic study on formaldehyde removal over Pd/TiO_2 catalysts: Oxygen transfer and role of water vapor. *Chem. Eng. J.* **2013**, *230*, 73−79.

(28) Chen, B.; Wang, B.; Sun, Y.; Wang, X.; Fu, M.; Wu, J.; Chen, L.; Tan, Y.; Ye, D. Plasma-Assisted Surface Interactions of Pt/CeO_2 Catalyst for Enhanced Toluene Catalytic Oxidation. *Catalysts* **2019**, *9*, 2.

(29) Zhou, J.; Wang, D.; Wu, G.; Fang, N.; Song, X.; Li, J.; Chen, J.; Liu, Y.; Guo, J.; Chu, Y. Enhanced Catalytic Combustion Performance of Toluene over a Novel Co-CeO_x Monolith Catalyst. *Energy Fuels* **2021**, *35*, 6190−6201.

(30) Hyok Ri, S.; Bi, F.; Guan, A.; Zhang, X. Manganese-cerium composite oxide pyrolyzed from metal organic framework supporting palladium nanoparticles for efficient toluene oxidation. *J. Colloid Interface Sci.* **2021**, *586*, 836−846.

(31) Xiaoyu, W.; Bingqing, S.; Annai, L.; Jingya, S.; Yan, X.; Haiqin, W.; Shourong, Z.; Lin, D.; Yu-wen, C. Highly dispersed Pd/modified-Al_2O_3 catalyst on complete oxidation of toluene: Role of basic sites and mechanism insight. *Appl. Surf. Sci.* **2019**, *497*, No. 143747.

(32) Trung, B. C.; Tu, L. N. Q.; Thanh, L. D.; Van Dung, N.; An, N. T.; Long, N. Q. Combined adsorption and catalytic oxidation for low-temperature toluene removal using nano-sized noble metal supported on ceria-granular carbon. *J. Environ. Chem. Eng.* **2020**, *8*, No. 103546.

(33) Qiao, N.; Li, Y.; Li, N.; Zhang, X.; Cheng, J.; Hao, Z. High performance Pd catalysts supported on bimodal mesopore silica for the catalytic oxidation of toluene. *Chin. J. Catal.* **2015**, *36*, 1686−1693.

(34) Du, X.; Dong, F.; Tang, Z.; Zhang, J. Precise design and synthesis of Pd/InO_x@CoO_x core-shell nanofibers for the highly efficient catalytic combustion of toluene. *Nanoscale* **2020**, *12*, 12133−12145.

https://doi.org/10.1021/acsomega.2c04331
ACS Omega 2022, 7, 39950−39958